Giant and tunable out-of-plane spin polarization of topological antimonene

Polina M. Sheverdyaeva[1,*¶], Conor Hogan[2,3*¶], Gustav Bihlmayer[4], Jun Fujii[5], Ivana Vobornik[5], Matteo Jugovac[1,6], Asish K. Kundu[1,7], Sandra Gardonio[8], Zipporah Rini Benher[8], Giovanni Di Santo[9], Sara Gonzalez[9], Luca Petaccia[9], Carlo Carbone[1], and Paolo Moras[1]

[1]*Istituto di Struttura della Materia-CNR (ISM-CNR), Strada Statale 14 km 163.5, 34149, Trieste, Italy*

[2] *Istituto di Struttura della Materia-CNR (ISM-CNR), Via del Fosso del Cavaliere 100, 00133 Roma, Italy*

[3] *Dipartimento di Fisica, Università di Roma "Tor Vergata", Via della Ricerca Scientifica 1, 00133 Roma, Italy*

[4]*Peter Grünberg Institut and Institute for Advanced Simulation, Forschungszentrum Jülich and JARA, D-52425 Jülich, Germany*

[5]*Istituto Officina dei Materiali (IOM)-CNR, Laboratorio TASC, Strada Statale 14 km 163.5, 34149, Trieste, Italy*

[6]*Peter Grünberg Institut PGI, Forschungszentrum Jülich, 52425 Jülich, Germany*

[7]*International Center for Theoretical Physics (ICTP), Trieste, 34151, Italy*

[8]*Materials Research Laboratory, University of Nova Gorica, Vipavska 11c, Ajdovščina 5270, Slovenia*

[9]*Elettra - Sincrotrone Trieste S.C.p.A., Strada Statale 14 km 163.5, 34149 Trieste, Italy*

Abstract

Topological insulators are bulk insulators with metallic and fully spin-polarized surface states displaying the Dirac-like band dispersion. Due to spin-momentum locking, these topological surface states (TSSs) have a predominant in-plane spin polarization in the bulk fundamental gap. Here, we show by spin-resolved photoemission spectroscopy that the TSS of a topological insulator interfaced with an antimonene bilayer exhibits a nearly full out-of-plane spin polarization within the substrate gap. We connect this phenomenon to a symmetry-protected band crossing of spin-polarized surface states. The nearly full out-of-plane spin polarization of the TSS occurs along a continuous path in the energy-momentum space, and the spin polarization within the gap can be reversibly tuned from nearly

full out-of-plane to nearly full in-plane by electron doping. These findings pave the way towards advanced spintronics applications that exploit the giant out-of-plane spin polarization of TSSs.

Keywords:

density functional theory, spin-resolved ARPES, electronic structure, topological insulators, 2D materials, antimonene

Topological insulators (TIs) are a class of materials with high spin-orbit coupling (SOC) and nontrivial band topology [1]. They are insulating in the bulk and metallic at the surfaces, due to the presence of robust Dirac-like topological surface states (TSSs) protected by time-reversal symmetry. TSSs are fully spin-polarized with a predominantly in-plane spin orientation near the Fermi level (E_F) as dictated by the symmetry of the spin-momentum locking. The charge-spin interconversion effects arising from this spin texture have remarkable applications in spintronics [2]. For example, injection of an electric current into a TI is known to generate in-plane spin transfer torques (STTs) orders of magnitude larger than in other materials with high SOC [3]. These giant STTs are suitable for low-power current-induced magnetization switching in TI/ferromagnetic layer hetero-structures [3].

A new spectrum of spintronic effects and related applications would open up if TIs with out-of-plane surface spin texture could be designed [4,5]. In the context of current-induced magnetization switching, out-of-plane STTs are expected to be more efficient than in-plane STTs in reversing the magnetization of layers with perpendicular magnetic anisotropy, which are typically used in logic and memory devices [6]. Nonetheless, to date only a few TSSs have shown significant out-of-plane spin polarization. Record values above 20% have been experimentally reported for Bi_2Te_3 [7], Sb_2Te_3 [8], $PbBi_2Te_4$ [9] and BiTeI [10], yet they remain much lower than the corresponding in-plane spin components. For this reason, phenomena associated with the out-of-plane spin polarization of the TSSs are still poorly explored experimentally [4,11].

The spin texture of a prototypical TI, Bi_2Se_3, was reported to be strongly modified upon the formation of an interface with a bilayer (BL) of honeycomb-like (β-)antimonene [12]. The topological proximity effect leads to a hybrid TSS that is confined within the antimonene BL and the topmost Se layer (hereon, TSS_{Sb}). A reverse of the in-plane spin texture and a significant out-of-plane spin polarization was noted in density functional theory (DFT) calculations [12]. Here, we provide for the first time a clear experimental demonstration of the phenomenon by means of spin- and angle-resolved

photoemission spectroscopy (spin-ARPES) and provide a quantitative, microscopic analysis of its origin using DFT. We show that the out-of-plane spin polarization of TSS_{Sb} reaches giant values of up to 94% within the substrate gap. We connect its emergence to a protected band crossing of fully polarized surface states along $\overline{\Gamma M}$. Similar band crossings of surface states were recently reported as two-dimensional analogs of tilted Weyl cones [13,14]. Importantly, the nearly full out-of-plane spin polarization of TSS_{Sb} is not limited to a certain direction but occurs among a wide range of wave vectors. We demonstrate that the degree of out-of-plane spin polarization of the TSS_{Sb} inside the Bi_2Se_3 gap can be finely and reversibly tuned by the adsorption of alkali metals or carbon oxide. We propose that similar spin textures may occur in other systems of hetero-structures comprising TIs, and that such interfaces can be seen as a viable way to tailor the out-of-plane spin texture of TIs.

We recall the electronic structure of the hetero-structure formed by one BL of antimonene (i.e., one layer of strongly buckled honeycomb-like β-antimonene [15]) and the Bi_2Se_3 substrate [12,16,17]. Figure 1(a) shows the calculated band structure along the $\overline{K\Gamma K}$ direction (k_x axis). The color scale indicates the spatial localization of the electronic states. Three bands are located within the fundamental gap of the substrate (gray dashed lines indicate the gap edges) [18]: P is localized in antimonene, TSS_{Sb} in antimonene and the topmost Se layer (Fig. 1(e), in close analogy to the case of Bi-terminated Bi_2Te_3 [19]), and B at the interface. TSS_{Sb} can be seen as the migration of the TSS of the substrate (TSS_{BS}) to the antimonene BL upon formation of the hetero-structure (topologization of antimonene by the proximity effect) [12, 16, 20]. The Dirac point D lies 0.2 eV above E_F in a local gap of the Bi_2Se_3 conduction band. The aforementioned three bands can be identified in the ARPES spectra of Fig. 1(b) ($h\upsilon$ = 14 eV). At this photon energy, the Bi_2Se_3-related spectral features are strongly suppressed thus allowing for a better visibility of antimonene-derived states (see for comparison Ref [12] and Fig. S1(a) of SM). TSS_{Sb} and B (green and light blue dashed lines) are in good agreement with the DFT calculations (see also Fig. S2(a,b) of SM and Ref [12]), while P (yellow dashed line) lies at higher binding energies than expected (Fig. S2(c,d) of SM). The gray dashed lines indicate the experimental position of the Bi_2Se_3 fundamental gap in the antimonene/Bi_2Se_3 hetero-structure (Fig. S1(a) of SM). TSS_{Sb} crosses the entire gap, and only the top part of B enters the gap. P lies below the bottom of the gap, where it overlaps and hybridizes with the Bi_2Se_3 states. Thus, the electronic and spin structure of the system within the fundamental gap of Bi_2Se_3 is determined by TSS_{Sb} and B, on which we focus from here onwards.

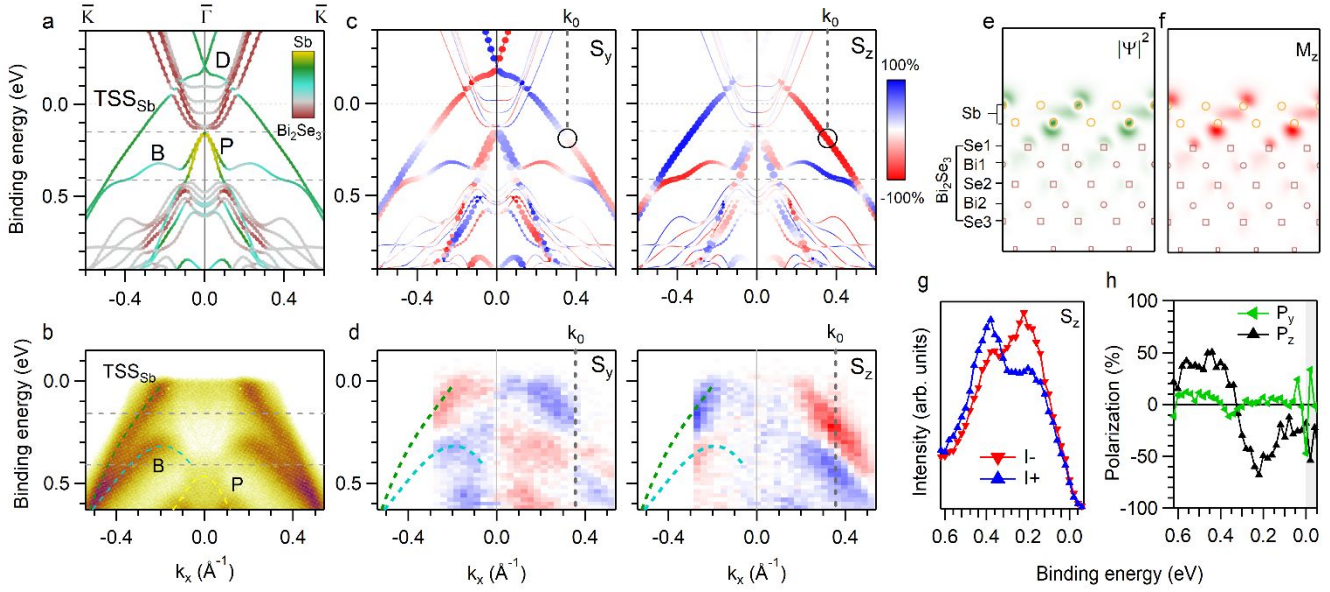

Fig. 1. Theoretical and experimental electronic structure of antimonene/Bi_2Se_3 along the $\overline{KΓK}$ direction. *(a) Band structure calculations. The color scale indicates the localization of the states. (b) ARPES data taken with* hν *= 14 eV. (c) Calculated in-plane (left) and out-of-plane (right) spin components. The size of the data points indicates the projection onto the Sb atoms. (d) Experimental in-plane (left) and out-of-plane (right) spin- and angle-resolved photoemission intensity measured with* hν *= 16 eV. (e) Charge density profile and (f) out-of-plane magnetization distribution of TSS_{Sb} (through the plane intersecting the Sb-Sb bond and topmost Se atom) at the position marked by a circle in panel (c). (g) Out-of-plane spin-resolved photoemission spectra taken at k_0. (h) Spin polarization spectra for the in-plane and out-of-plane spin components at k_0.*

Fig. 1(c) shows the calculated in-plane (S_y) and out-of-plane (S_z) spin components for the electronic states of antimonene/Bi_2Se_3. TSS_{Sb} is fully in-plane spin-polarized near D, in close analogy to the behavior of TSS_{BS} [21]. Its S_y component decreases steeply below D and reverses at $k_0 = 0.35$ Å^{-1} (black circle at 0.19 eV), in agreement with literature [12,16]. We analyzed quantitatively the S_z component of TSS_{Sb} at k_0 and observed a surprisingly high value close to 94%. It remains larger than S_y throughout the fundamental gap of Bi_2Se_3 and reaches about 57% at E_F. B shows a similar predominance of S_z over S_y, and an opposite spin texture with respect to TSS_{Sb}.

The spin-ARPES data of Fig. 1(d) confirm the predicted properties of TSS_{Sb} and B. The in-plane spin textures of TSS_{Sb} and B are reversed at k_0. At this point the out-of-plane spin polarization P_z is about

66% for TSS_{Sb} and 48% for B, and the in-plane ones are close to zero (Fig. 1(g,h) and Fig. S3(a) of SM). These as-measured out-of-plane spin polarizations are about twice larger than the so far experimentally reported values for the TSSs, despite being lower, as typically observed, than the theoretically predicted due to extrinsic and intrinsic effects [7,8,11]. While referring to the total spin polarization $P_{tot}=\sqrt{P_x^2+P_y^2+P_z^2}$, [8, 11], the P_z values at k_0 reach 99% and 98%, respectively, in very good agreement with the values predicted by DFT. The complete inversion of S_y and S_z textures at opposite k_x values (Fig. 1(d)) and the agreement with the DFT calculations show that the present measurements capture the spin polarization of TSS_{Sb} and B in the initial state [11, 22], which is the relevant property for spintronics. As expected from symmetry considerations, P_z is zero along $\overline{M\Gamma M}$ (Fig. S3(b) of SM).

The spin texture of TSS_{Sb} within the Bi_2Se_3 fundamental gap differs remarkably from that of other TSSs in the absolute size of the (giant) S_z values and in the predominance of S_z over S_y. For example, the predicted and measured S_z values for the TSSs of Bi_2Te_3 [7, 8] and $PbBi_2Te_4$ [9] are 30-40% and about 20%, respectively. In Bi_2Te_3, the out-of-plane spin component is very small at E_F, increases moving away from the Dirac point, and reaches its maximum above E_F [7]. In the case of antimonene/Bi_2Se_3, instead, S_z of TSS_{Sb} is giant within the substrate's gap and remains predominant between E_F and 0.5 eV. So far, giant S_z values have been reported only for the states of transition metal dichalcogenides [23,24] or Bi films [25], which lack topological protection [26]. Another important difference with respect to these materials concerns the spatial properties of TSS_{Sb} where S_z is maximal (circle in Fig. 1(c)). Here, TSS_{Sb} displays a high surface localization (Fig. 1(e)) and a uniform orientation of the magnetization pattern (Fig. 1(f)), whereas the magnetization pattern in WSe_2 and Bi_2Te_3 switches from positive to negative moving from one atomic plane to the next [7, 24, 27]. This high surface spin localization and absence of the spin reversal may lead to large spin decoherence times, which are appealing for spintronic applications [7, 28].

In order to explore the origin of the unusually high S_z values of TSS_{Sb} and B we followed the evolution of their spin texture by artificially increasing the distance between antimonene and Bi_2Se_3 (Fig. S4 of SM). The calculated S_z is weak in both nearly free-standing antimonene and Bi_2Se_3, and therefore the observed giant S_z is an exclusive property of the hetero-structure. In contrast to WSe_2, where states with dominant d_z^2/p_z character exhibit strongly suppressed S_z [24], the charge density profile has a dominant p_z component [16] that hardly changes as a function of distance (Fig. S5 of SM). According to Ref [29], the presence of an in-plane electric field can also give rise to a high S_z. We analyzed different

stacking arrangements of antimonene and Bi_2Se_3 atomic layers (Fig. S6 of SM) and found that the out-of-plane spin texture is reversed only when the *substrate* stacking--and thus the local potential gradient--is modified. However, since the out-of-plane electric field is normally much larger than the in-plane one, these results would not explain the unusually high, almost fully out-of-plane spin polarization.

In Fig. 2 we demonstrate that the giant S_z values of TSS_{Sb} and B derive from the constraint imposed by mirror symmetry on their in-plane spin texture. Fig. 2(a) shows the band structure of the hetero-structure along $\overline{\Gamma M}$ direction. We can observe TSS_{Sb} and B bands that cross close to 0.25 eV binding energy. The top (bottom) row of Fig. 2(b) shows the in-plane (out-of-plane) spin components of TSS_{Sb} and B along radial axes comprised between $\overline{\Gamma M}$ and $\overline{\Gamma K}$. Since the spin projection along the wave vector direction is forbidden by the symmetry of the Rashba model [30], the sum of the spin components shown in the top and bottom rows is always 100% for every state. In particular, along $\overline{\Gamma M}$ both states are fully in-plane spin-polarized. Similar band crossing of fully-polarized surface states were recently reported experimentally and referred to as two-dimensional analogs of tilted Weyl cones [13,14]. The mirror symmetry along $\overline{\Gamma M}$ protects their accidental crossing from opening a gap. Moving away from $\overline{\Gamma M}$ towards $\overline{\Gamma K}$ the symmetry constraint vanishes and a gap can open (see Fig. S7 of SM). Since the spin texture of the bands far from the gap region is maintained, the in-plane spin component is forced to become zero while approaching the gap (top row). This results in the emergence of nearly full out-of-plane spin components with opposite sign for TSS_{Sb} and B (bottom row). We emphasize that TSS_{Sb} and B display giant S_z not only along $\overline{\Gamma K}$ but everywhere in the momentum space, except along the six $\overline{\Gamma M}$ axes. This is qualitatively different from the S_z of TSSs of TIs, related to their hexagonal warping, that reaches maximum along $\overline{\Gamma K}$. The points where S_z is maximal, i.e. close to 100%, (two gray circles mark these points in the central panels of Fig. 2(b), as an example) form the two wavy contours displayed in Fig. 2(c). Importantly, they are fully located within the bulk band gap of the substrate.

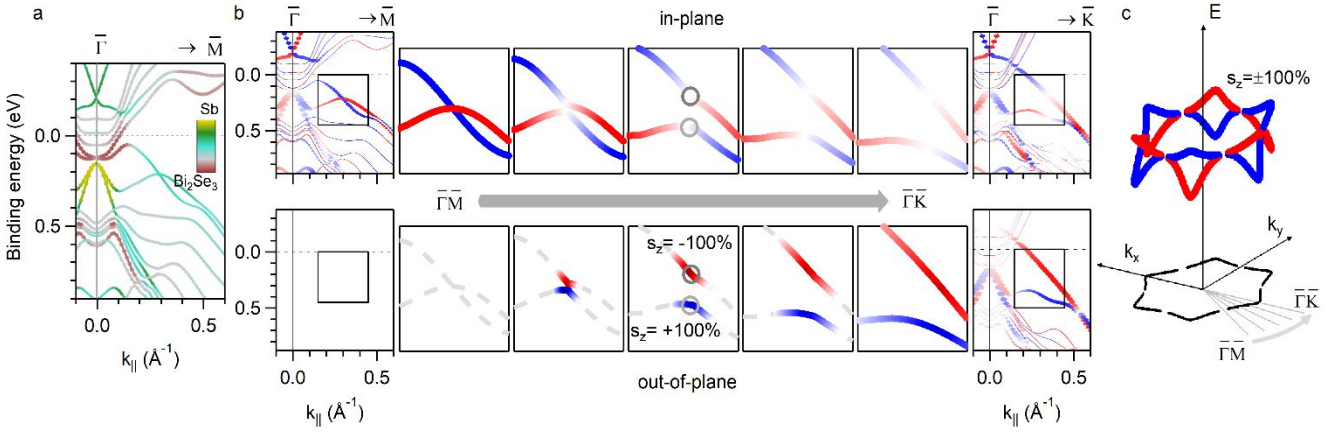

Fig. 2. Origin of the giant out-of-plane spin texture. *(a) Band structure calculations along $\overline{\Gamma M}$. The color scale indicates the localization of the states. (b) Spin-resolved band structure. Top row: in-plane spin component of the TSS_{Sb} and B bands along radial axes comprised between $\overline{\Gamma M}$ and $\overline{\Gamma K}$. Bottom row: same as the top row for the out-of-plane spin component. Gray circles mark the states with zero in-plane and ±100% out-of-plane spin component in the central panels. Band dispersions away from high symmetry directions are shown schematically. (c) Schematic representation of the S_z=±100% contours for TSS_{Sb} and B in the energy-momentum space.*

We now explore the possibility of tuning the out-of-plane spin texture of antimonene/Bi_2Se_3 by electron doping. Fig. 3(a) shows the band structure of the system with 0.25 monolayer (ML) of K on top of antimonene in the most stable atomic configuration (Section 2 of SM, Fig. S8–S10 and Table S1 consider other structures and coverages). Here, 1 ML corresponds to the density of the uppermost Sb plane. The K-induced electron doping influences differently the antimonene- and Bi_2Se_3-related features due to the presence of a surface dipole (Fig. S11 of SM). D is shifted towards higher binding energy by 0.7 eV (green arrow at 0.5 eV below E_F) and the bulk Bi_2Se_3 bands by only 0.3 eV. This relative energy shift strongly alters the spin texture of the system (Fig. 3(b)). Now TSS_{Sb} shows pronounced S_y and negligible S_z components within the entire fundamental gap of Bi_2Se_3 (B becomes degenerate with the bulk valence states of the Bi_2Se_3). This behavior is expected on the basis of the spin structure of TSS_{Sb} above D (Fig. 1(c)) and the analogous relative shift between TSS_{BS} and the bulk

bands observed upon alkali metal deposition on Bi_2Se_3 [31-33]. Notably, TSS_{Sb} retains the strongly localized character (Fig. 3(c)) and the constant out-of-plane magnetization pattern (Fig. 3(d)) of the pristine antimonene/Bi_2Se_3 system.

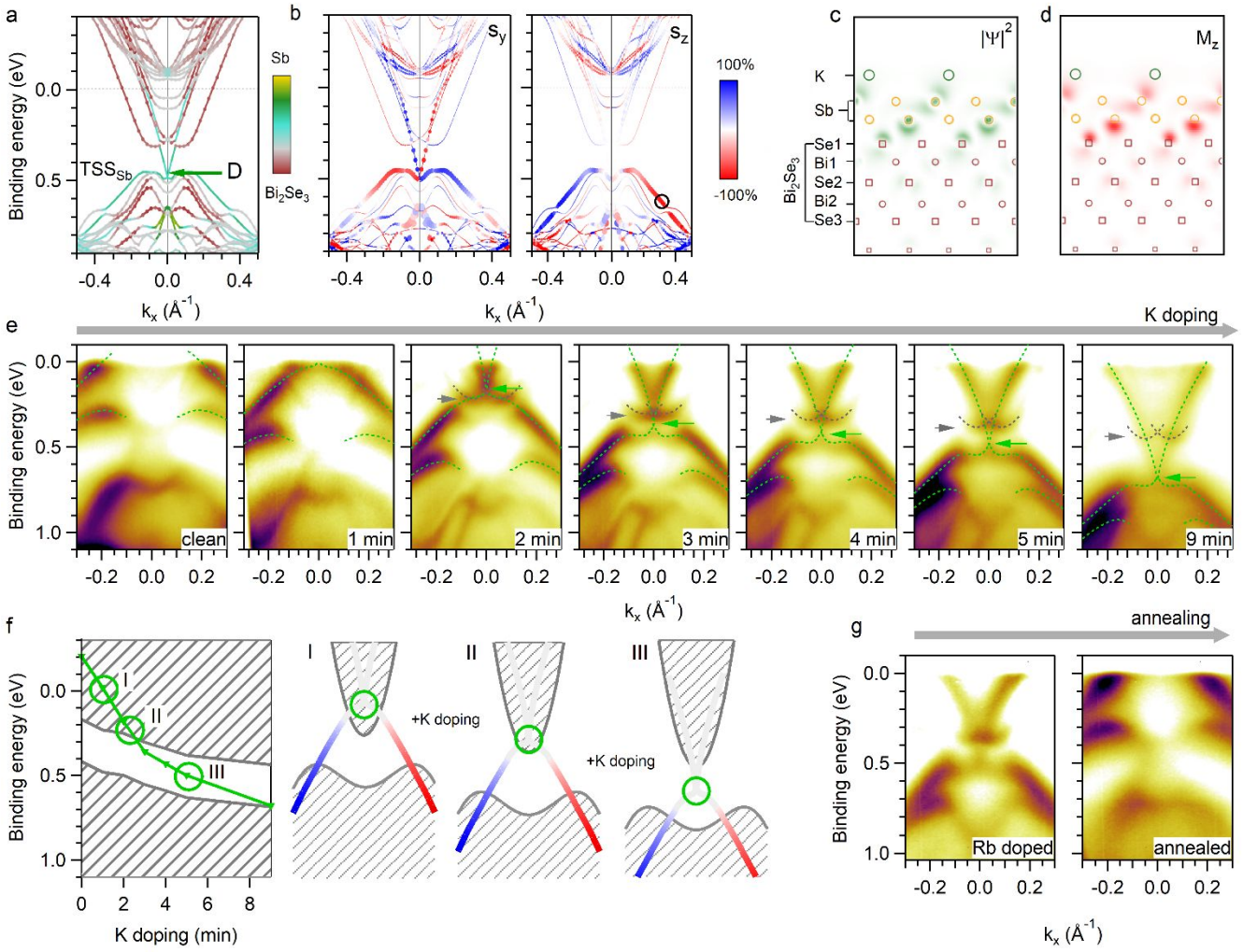

Fig. 3. Tailoring of the spin texture by electron doping. *(a) Band structure calculations for 0.25 ML K/antimonene/*Bi_2Se_3*. The color scale indicates the localization of the states. (b) Calculated in-plane (left) and out-of-plane (right) spin components. The size of the data points indicates the projection onto the Sb atoms. (c) Charge density profile and (d) out-of-plane magnetization distribution of* TSS_{Sb} *at the position marked by a circle in panel (b). (e) ARPES spectra along* $\overline{K\Gamma K}$ *as a function of the K coverage, hυ=14 eV. (f) Position of D (green) with respect to the bulk band edges (gray) and the schematics of the out-of-plane spin texture of* TSS_{Sb} *as a function of the K deposition; (g) ARPES spectra of antimonene/*Bi_2Se_3 *doped by Rb before and after annealing to 85°C.*

The electronic structure shown of Fig. 3(a) is actually observed by ARPES when K is deposited on the surface of antimonene/Bi_2Se_3 (Fig. 3(e)). As the amount of K increases, TSS_{Sb} and B (green dashed lines) continuously shift towards higher binding energies. D (green arrow) becomes visible from 2 min. deposition and reaches 0.7 eV at saturation coverage. Starting from the 2 min. deposition, we also observe two inverted parabolas (grey dashed lines) that shift towards higher binding energy as the K doping increases (Fig. S1(b-d) of SM). By comparison with the calculations of Fig. 3(a) and the ARPES data of K-doped Bi_2Se_3 [31], these bands can be identified with the bottom of the bulk conduction band of Bi_2Se_3. Since the size of the fundamental gap of Bi_2Se_3 is known (0.25 eV), it is possible to locate D with respect to the bulk band edges at each K deposition step, as shown in the left side of Fig. 3(f). The resulting electronic structure of the system, regarding TSS_{Sb} only, is schematically shown in the right side of Fig. 3(f). In pristine or lightly K-doped antimonene/Bi_2Se_3 (I), the spin texture in the fundamental gap of Bi_2Se_3 is dominated by states with giant S_z. With increasing the K coverage, the S_z component of TSS_{Sb} decreases (II) and eventually disappears (III).

A similar electron doping effect can be induced by dosing Rb or CO on antimonene/Bi_2Se_3 held at liquid nitrogen temperature (left side of Fig. 3(g) and Fig. S12 of SM). Also in this case, we observe the downward shift of TSS_{Sb} and B and the appearance of two inverted parabolas, in close analogy to the K-doped system. Similarly to Bi_2Se_3 [31], the effect of K, Rb and CO dosing can be removed by raising the temperature of the antimonene/Bi_2Se_3 system, thus making the electron doping effect largely reversible (right side of Fig. 3(g) and Fig. S12 of SM).

Our analysis demonstrates that it is possible to design topological systems with giant S_z components by interfacing existing TIs with trivial materials, such as semiconducting antimonene. The antimonene/Bi_2Se_3 hetero-structure features a single spin channel inside the bulk gap with a giant out-of-plane spin polarization and topological protection, which is strongly localized in the surface. This system satisfies an important requirement for spintronic applications, i.e. the tunability of spin- and electronic properties [34-37]. The out-of-plane spin polarization can indeed be finely and reversibly tuned from almost 100% to 0%. This final state can also be reached via absorption of other elements, such as Mg and Ca [38]. The simple band structure described above can be used as a model for simulation and experimental testing of transport properties for spintronic devices and could be implemented in magnetic memory applications.

The mechanism described above, in which a fully out-of-plane spin polarization arises from a symmetry-protected Weyl-like band crossing, has so far not been proposed. We suggest that it may manifest in other systems that feature a protected band crossing along a line of mirror symmetry. In the context of topologically protected states, a band crossing along the $\overline{\Gamma M}$ direction and exhibiting a similar in-plane spin texture reversal, was observed in the related system of double BL antimonene on Bi_2Se_3 [12]. A protected band crossing followed by a nearly full S_z may well exist also in similar hetero-structures that manifest a topological proximity effect, i.e. antimonene on Bi_2Te_3, Sb_2Te_3 and Bi_2Se_2Te [16,39,40]. A crossing of spin-polarized surface bands along a high symmetry line was experimentally reported for NbGeSb [13] and W(110) [14]. Although these states lack topological protection, one may also expect a full out-of-plane spin polarization away from mirror symmetry planes in these systems.

Methods

High quality single crystals of Bi_2Se_3 were grown by the Bridgman method. Bismuth and selenium were purchased from Sigma Aldrich at 99.999% and ≥99.5% trace metal basis respectively. The stoichiometric amounts of high purity elements were sealed in evacuated quartz ampoules and heated up to 750°C at 21 °C/h. The ampoules were maintained at that temperature for 48 h. Thereupon the temperature was slowly reduced to 250°C at 5 °C/h and then cooled down to room temperature.

Sb was deposited on freshly cleaved Bi_2Se_3 at room temperature and subsequently annealed to 430 K to form the β-antimonene phase as described in Refs. [12,17,41]. Potassium and rubidium were deposited on the sample kept at 80 K at a rate of 0.04 monolayer (ML)/min (as referred to the density of the Bi_2Se_3 surface). CO adsorption was achieved by cooling the sample from room temperature to 80 K in a CO atmosphere. The LEED pattern showed sharp 1×1 spots at all preparation stages (Fig. S13 of SM).

DFT calculations were performed within a plane-wave/pseudopotential framework as implemented in the quantum-ESPRESSO (QE) code [42]. Spin-orbit coupling was incorporated via use of fully relativistic ultrasoft pseudopotentials [43,44] with a kinetic energy cutoff of 45 Ry. The Bi_2Se_3 surface was modeled using a centrosymmetric slab containing six quintuple layers. The four topmost atomic layers (plus the antimonene layer and the K atoms) were allowed to relax during structural optimization. The experimental lattice constant of 4.143Å was used [45]. The PBE functional [46] and Grimme-D2 van der Waals correction [47] were adopted. This computational scheme yielded results in

close agreement with our previous studies using QE and VASP [12,17]. The equilibrium distance d_0 = 2.32 Å and the 1×1 lattice matching considered in the calculations are justified in previous structural studies of the system [12,20]. Adsorption of potassium was simulated using 1×1, 2×2, and 3×3 supercells, corresponding to coverages of 1, 0.25, and 0.11 ML. Several on-top and intercalated geometries were investigated, as shown in Section 2 of SM.

The ARPES experiments were carried out at the APE-LE [48], BaDElPh [49] and VUV-Photoemission beamlines of the synchrotron Elettra (Trieste, Italy) with hυ = 14–60 eV and *p*-polarized light at 77 K. The electron spectrometers were placed at an angle between 42° and 50°, with reference to the direction of the incoming *p*-polarized photon beam. The energy resolution was of about 20 meV, and momentum resolution of about 0.02 $Å^{-1}$. Spin-resolved ARPES data were taken at APE-LE beamline, by using a Scienta-Omicron DA30 hemispherical analyzer operating in the deflection mode and equipped with two orthogonal VLEED reflectometers, with energy resolutions of about 90 meV, and momentum resolution of about 0.04 $Å^{-1}$. During the spin measurements, the analyser's slits were set parallel to the $\overline{KΓK}$ direction, the spin-ARPES spectra along high symmetry directions were obtained by using the deflectors without moving the sample. The spin-polarization was calculated as described in Ref [48] and using the Sherman function value S = 0.26.

Data availability

The data that support the findings of this study are available within the article and Supplementary Information. Extra data are available from the corresponding authors upon reasonable request.

Supporting information

Additional experimental data (ARPES and spin-ARPES data, LEED patterns) as well as DFT calculations useful to understand the theoretical results shown in the main text (PDF)

Author Information

Corresponding Author

* Polina M. Sheverdyaeva, Email: polina.sheverdyaeva@ism.cnr.it

* Conor Hogan, Email: conor.hogan@ism.cnr.it

ORCID

Polina M. Sheverdyaeva 0000-0002-4231-1638

Conor Hogan 0000-0002-0870-6361

Gustav Bihlmayer 0000-0002-6615-1122

Jun Fujii 0000-0003-3208-802X

Ivana Vobornik 0000-0001-9957-3535

Matteo Jugovac 0000-0001-9525-3980

Asish K. Kundu 0000-0003-2199-1053

Sandra Gardonio 0000-0002-5560-718X

Zipporah Rini Benher 0000-0003-3923-750X

Giovanni Di Santo 0000-0001-9394-2563

Sara Gonzalez 0000-0002-7698-3539

Luca Petaccia 0000-0001-8698-1468

Carlo Carbone 0000-0002-8675-7850

Paolo Moras 0000-0002-7771-8737

Author Contributions

¶ P.M.S. and C.H. contributed equally to this work

Present Address

Sara Gonzalez: Institut des nanotechnologies de Lyon, Lyon, France

Matteo Jugovac: Elettra - Sincrotrone Trieste S.C.p.A., Strada Statale 14 km 163.5, 34149 Trieste, Italy

Asish K. Kundu: National Synchrotron Light Source, Brookhaven National Laboratory, Upton, New York 11973, USA

Acknowledgements

We acknowledge EUROFEL-ROADMAP ESFRI of the Italian Ministry of Education, University, and Research. A.K.K. acknowledges receipt of a fellowship from the ICTP-TRIL Programme, Trieste, Italy. We acknowledge Elettra Sincrotrone Trieste for providing access to its synchrotron radiation facilities. C.H. acknowledges CINECA under the ISCRA initiative for availability of high-performance computing resources and support.

References

[1] Zhang, H. et al. Topological insulators in Bi2Se3, Bi2Te3 and Sb2Te3 with a single Dirac cone on the surface. *Nat. Phys.* **2009**, *5*, 438–442.

[2] Zhang, S. & Fert A. Conversion between spin and charge currents with topological insulators. *Phys. Rev. B* **2016**, *94,* 184423.

[3] Mellnik, A. R. et al. Spin-transfer torque generated by a topological insulator. *Nature* **2014**, *511,* 449–451.

[4] Han, J. & Liu, L. Topological insulators for efficient spin–orbit torques. *APL Materials* **2021**, *9*, 060901.

[5] Liu, Y. & Shao, Q. Two-Dimensional Materials for Energy-Efficient Spin–Orbit Torque Devices. *ACS Nano* **2020**, *14* (8), 9389–9407.

[6] Ikeda, S. et al. A perpendicular-anisotropy CoFeB–MgO magnetic tunnel junction. *Nat. Mater.* **2010**, *9*, 721–724.

[7] Herdt, A. et al. Spin-polarization limit in Bi2Te3 Dirac cone studied by angle- and spin-resolved photoemission experiments and ab initio calculations. *Phys. Rev. B* **2013**, *87*, 035127.

[8] Nomura, M. et al. Relationship between Fermi surface warping and out-of-plane spin polarization in topological insulators: A view from spin- and angle-resolved photoemission. *Phys. Rev. B* **2014**, *89*, 045134.

[9] Eremeev, S.V. et al. Atom-specific spin mapping and buried topological states in a homologous series of topological insulators. *Nat. Commun.* **2012**, *3*, 635.

[10] Sakano, M. et al. Strongly Spin-Orbit Coupled Two-Dimensional Electron Gas Emerging near the Surface of Polar Semiconductors. *Phys. Rev. Lett.* **2013**, *110*, 107204.

[11] Dil, J. Hugo. Spin- and angle-resolved photoemission on topological materials. *Electron. Struct.* **2019**, *1*, 023001.

[12] Holtgrewe, K. et al. Topologization of β-antimonene on Bi2Se3 via proximity effects, *Scientific Reports* **2020***, 10*, 14619.

[13] Marković, I. et al. Weyl-like points from band inversions of spin-polarised surface states in NbGeSb. *Nat. Commun.* **2019**, *10*, 5485.

[14] Varykhalov, A. et al. Tilted Dirac cone on W(110) protected by mirror symmetry. *Phys. Rev. B* **2017**, *95*, 245421.

[15] Aktürk, O. Ü., Özçelik, V. O. & Ciraci, S. Single-layer crystalline phases of antimony: Antimonenes. *Phys. Rev. B* **2015**, *91*, 235446.

[16] Jin, K.-H.., Yeom, H. W., & Jhi, S.-H. Band structure engineering of topological insulator heterojunctions. *Phys. Rev. B* **2016**, *93*, 075308.

[17] Flammini, R. et al. Evidence of β-antimonene at the Sb/Bi2Se3 interface. *Nanotechnology* **2018**, *29*, 065704.

[18] Nechaev, I. A. et al. Evidence for a direct band gap in the topological insulator Bi2Se3 from theory and experiment. *Phys. Rev. B* **2013**, *87*, 121111.

[19] Hirahara, T. et al. Interfacing 2D and 3D Topological Insulators: Bi(111) Bilayer on Bi2Te3. *Phys. Rev. Lett.* **2011**, *107*, 166801.

[20] Holtgrewe, K., Hogan, C. & Sanna, S. Evolution of Topological Surface States Following Sb Layer Adsorption on Bi2Se3. *Materials* **2021**, *14*, 1763.

[21] Hsieh, D. et al. A tunable topological insulator in the spin helical Dirac transport regime. *Nature* **2009**, *460*, 1101.

[22] Bigi, C. et al. Measuring spin-polarized electronic states of quantum materials: 2H-NbSe2. *Phys. Rev. B* **2021**, *103*, 245142.

[23] Bawden, L. et al. Spin–valley locking in the normal state of a transition-metal dichalcogenide superconductor. *Nat. Commun.* **2016***, 7*, 11711.

[24] Riley, J. M. et al. Direct observation of spin-polarised bulk bands in an inversion-symmetric semiconductor. *Nat. Phys.* **2014**, *10*, 835–839.

[25] Takayama, A., Sato, T., Souma, S. & Takahashi, T. Giant Out-of-Plane Spin Component and the Asymmetry of Spin Polarization in Surface Rashba States of Bismuth Thin Film. *Phys. Rev. Lett.* **2011**, *106*, 166401.

[26] Aguilera, I., Kim, H.-J., Friedrich, C., Bihlmayer, G. & Blügel, S. Z2 topology of bismuth. *Phys. Rev. Mat.* **2021**, *5*, L091201.

[27] Henk, J., Ernst, A., Eremeev, S.V., Chulkov, E. V., Maznichenko, I. V., & Mertig, I. Complex Spin Texture in the Pure and Mn-Doped Topological Insulator Bi2Te3. *Phys. Rev. Lett.* **2012**, *108*, 206801.

[28] Schliemann, J. Colloquium: Persistent spin textures in semiconductor nanostructures. *Rev. Mod. Phys.* **2017**, *89*, 011001.

[29] Friedrich, R., Caciuc, V., Bihlmayer, G., Atodiresei N., & Blügel, S. Designing the Rashba spin texture by adsorption of inorganic molecules. *New J. Phys.* **2017**, *19*, 043017.

[30] Bychkov, Y. A., & Rashba, É. I. (1984). Properties of a 2D electron gas with lifted spectral degeneracy. *JETP Lett.* **1984**, *39*, 78.

[31] Zhu, Z.-H. et al. Rashba Spin-Splitting Control at the Surface of the Topological Insulator Bi_2Se_3. *Phys. Rev. Lett.* **2011**, *107*, 186405.

[32] Bianchi, M., Hatch, R. C., Mi, J., Iversen, B. B. & Hofmann, P. Simultaneous quantization of bulk conduction and valence states through adsorption of nonmagnetic impurities on Bi_2Se_3. *Phys. Rev. Lett.* **2011**, *107*, 086802.

[33] Förster, T., Krüger, P., & Rohlfing, M. Ab initio studies of adatom- and vacancy-induced band bending in Bi_2Se_3. *Phys. Rev. B* **2015**, *91*, 035313.

[34] Kondou, K. et al. Fermi-level-dependent charge-to-spin current conversion by Dirac surface states of topological insulators. *Nat. Phys.* **2016**, *12*, 1027–1031.

[35] Su, S. H. et al. Topological Proximity-Induced Dirac Fermion in Two-Dimensional Antimonene. *ACS Nano* **2021**, *15*, 15085–15095.

[36] Sun, R. et al. Large Tunable Spin-to-Charge Conversion Induced by Hybrid Rashba and Dirac Surface States in Topological Insulator Heterostructures. *Nano Lett.* **2019**, *19*, 4420–4426.

[37] Barfuss, A. et al. Elemental Topological Insulator with Tunable Fermi Level: Strained α-Sn on InSb(001). *Phys. Rev. Lett.* **2013**, *111*, 157205.

[38] Upadhyay, S. and Srivastava, P. DFT study of adsorption and diffusion of Mg, K, Ca over monolayer antimonene. *IOP Conf. Ser.: Mater. Sci. Eng.* **2021**, *1120*, 012035.

[39] Lei, T. et al. Electronic structure of antimonene grown on Sb_2Te_3 (111) and Bi_2Te_3 substrates. *J. Appl. Phys.* **2016**, *119*, 015302.

[40] Lei, T. et al. Electronic states driven by the crystal field in two-dimensional materials: The case of antimonene *Physical Review B* **2022**, *105*, 115404.

[41] Hogan, C. et al. Temperature Driven Phase Transition at the Antimonene/Bi2Se3 van der Waals Heterostructure. *ACS Nano* **2019**, *13*, 10481−10489.

[42] Giannozzi, P. et al. QUANTUM ESPRESSO: a modular and open-source software project for quantum simulations of materials. *J. Phys.: Condens. Matter* **2009**, *21*, 395502.

[43] Dal Corso, A. & Mosca Conte, A. Spin-orbit coupling with ultrasoft pseudopotentials: Application to Au and Pt. *Phys. Rev. B* **2005**, *71*, 115106.

[44] Dal Corso, A. Pseudopotentials periodic table: From H to Pu. *Comput. Mater. Sci.* **2014**, *95*, 337.

[45] Nakajima, S. The crystal structure of $Bi_2Te_{3-x}Se_x$. J. *Phys. Chem. Solids* **1963**, *24*, 479.

[46] Perdew, J. P., Burke, K. & Ernzerhof, M. Generalized Gradient Approximation Made Simple. *Phys. Rev. Lett.* **1996**, *77*, 3865.

[47] Grimme, S. J. Semiempirical GGA-type density functional constructed with a long-range dispersion correction. *Comput. Chem.* **2006**, *27*, 1787.

[48] Bigi, C. et al. Very efficient spin polarization analysis (VESPA): new exchange scattering-based setup for spin-resolved ARPES at APE-NFFA beamline at Elettra. *J. Synchrotron Radiat.* **2017**, *24*, 750.

[49] Petaccia, L. et al. BaD ElPh: A 4 m normal-incidence monochromator beamline at Elettra. *Nucl. Inst. Meth. Phys. Res.* A **2009**, *606*, 780.

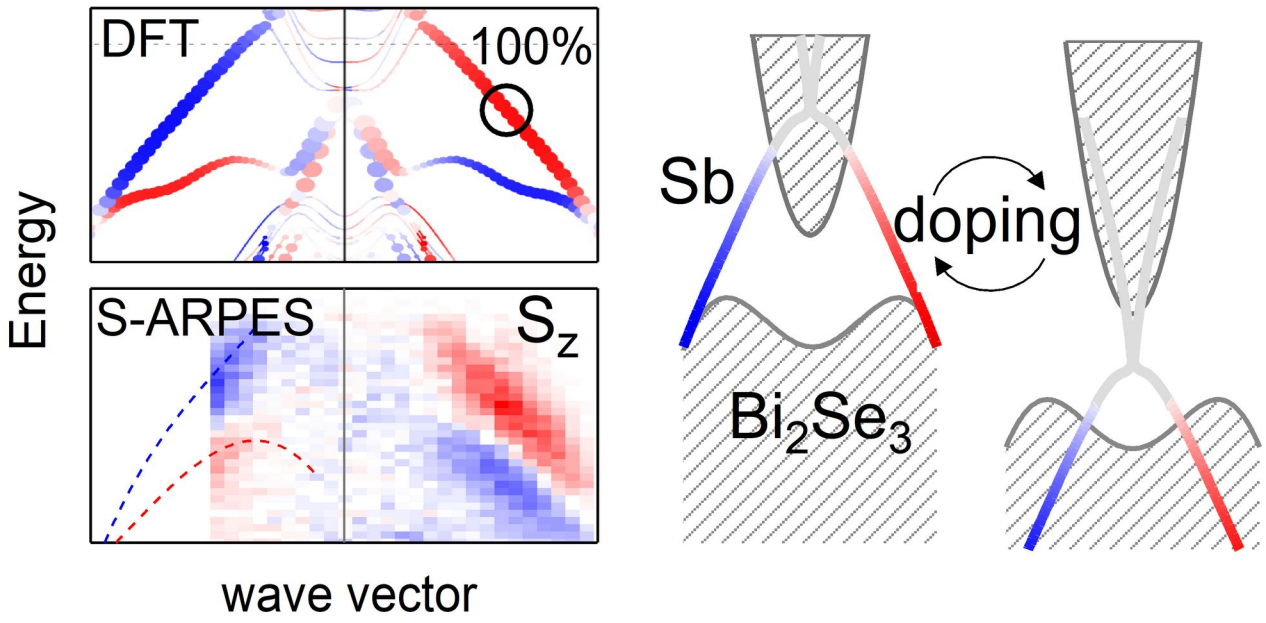

TOC graphic